A Novel Model of Influence Function: Calibration of a Continuous Membrane Deformable Mirror

M. B. Roopashree[1], Akondi Vyas[1,2], and B. Raghavendra Prasad[2]
[1] Indian Institute of Astrophysics, Bangalore, India
Email: brp@iiap.res.in
[2] Indian Institute of Science, Bangalore, India

***Abstract*—Measurement and modeling of the influence function plays a vital role in assessing the performance of the continuous MEMS deformable mirror (DM) for adaptive optics applications. The influence function is represented in terms of Zernike polynomials and shown that the dominant modes for representation of central actuators of the DM are different from those for the edge actuators. In this paper, a novel and effective method of modeling the influence function for all the DM actuators is proposed using the 2D sinc-squared function.**

***Index Terms*—deformable mirror, influence function, adaptive optics**

I. Introduction

Deformable mirrors (DMs) are adaptive devices capable of correcting the dynamic effects on optical wavefronts due to random processes, in the likes of atmospheric turbulence. These are often used in adaptive optics systems and are commonly controlled by the application of forces on actuators that hold the mirror surface. Two kinds of DMs are available – segmented and continuous. Unlike the discrete actuators holding individual mirror segments in the segmented DM case, the later uses a continuous membrane. Minimal edge diffraction in the case of a continuous DM makes it more desirable of the two. Since in most applications, the wavefronts to be corrected by the DM are often much smoother than the resolution limit of the device, it is advantageous to use the continuous DM with precise calibration [1-3]. The effect of individual actuators is desired to be localized, but, in the case of a continuous DM, the application of a certain force on one of the actuators results in a finite displacement (that cannot be neglected) at the neighboring actuator location. This error due to non-localized actuation can be largely compensated by determining the influence function, which is a measure of the response of the DM surface when a known voltage (called poke voltage) is applied to a single DM actuator (a constant bias voltage is applied to all the other actuators). The motive of the present work is to construct a mathematical model for the measured influence function.

Two other metrics used for the assessment of the DM performance include, the inter-actuator coupling coefficient and the interaction matrix. The inter-actuator coupling coefficient is defined as the ratio of the displacement of the DM surface at the poked actuator to that obtained at its neighboring actuator. It is often practically convenient to employ the interaction matrix, that relates the wavefront sensor measurements and the weighting associated with the basis functions used to fit the wavefront shape on the DM, to account for the actuator coupling [4].

Obtaining a fit function for the measured influence function for all the actuators individually can be useful in accurately modeling the DM. Most researchers use a Gaussian model,

$$IF(x, y) = a + b\ \exp\left\{-(w_x x^2 + w_y y^2)\right\} \quad (1)$$

which is not a true representation of the influence function. The outer portion of the influence function is different from a Gaussian as was pointed out by Wenhan Jiang, et. al. [5]. With azimuthal and radial modification to the Gaussian function, the influence function can be modeled more accurately [6]. But, it should be noted that the edge actuators are poorly modeled by the earlier suggested models. J. H. Lee, et. al [7] used the 1D sinc function to model the 1D influence function. In this paper, it is shown that the 2D sinc-squared function and Zernike moments can be used to effectively model the influence function. The measurements were made using the Shack Hartmann Wavefront Sensor (SHWS) for all the actuators. The SHWS measures the local slopes of the incident wavefront (in terms of the shift in the focal spots of the microlenses from ideal positions) and the shape of the wavefront is calculated using the least square techniques.

In our study, the Multi-DM, manufactured by Boston Micromachine Corporation (BMC) was used. The following section discusses the method used for the measurement of the influence function. Evaluation of the inter-actuator coupling is presented in section III. Section IV details the modeling of the influence function.

II. Influence Function Measurement

A. Experimental details

The optical arrangement for the measurement of the DM influence function is shown in Fig. 1. A 15mW Melles Griot He-Ne laser was used as the source of light. The laser beam was filtered using the spatial filter (S.F) and then collimated with a doublet lens (CL). The beam was allowed to reflect from the DM surface. The beam was then filtered using the 4f lens geometry (L_1, L_2 are equi-focal lenses, f=12.5cm). The assembled SHWS was made-up of a contiguous microlens array (from Flexible Optical BV, APO-Q-P200-F40 at 633nm, with a focal length of f=40mm and a pitch of p=200μm) and a compact, high-resolution progressive monochrome CCD

DOI: 01.IJCSI.03.02.49

camera (Pulnix TM-1325CL). The camera was placed at the focal plane of the microlens array (a distance f=4cm away). It is important to note here that the performance of the SHWS is highly sensitive to placing the CCD at the focal plane of the microlenses [8].

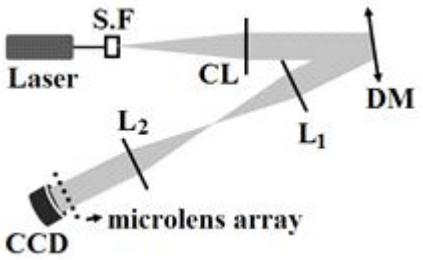

Figure 1. Optical arrangement for the measurement of the DM influence function

In view of the fact that the clear aperture on the DM is 4.9×4.9 mm^2 and the pitch of the microlens array is 200μm, 25×25 microlenses were used to incorporate the entire active region of the DM, for sensing. Also, the pitch of the CCD pixels is 6.45μm, which implies that a single mircolens corresponds to 31 pixels on the CCD, given the pitch of the microlens array to be 200μm. For the reason that, the light levels and frame rates are not the points of concern, the high readout noise (50 e^- per frame per pixel) is not an issue in our case [9]. In contrary, the high resolution of the camera provides high-quality, accurate wavefront sensing capabilities. The maximum voltage that was applied to the DM actuators was limited to 40V to avoid SHWS cross-talk. The 140 actuators of the DM are numbered as shown in Fig. 2 (when quoted, they are written in bold throughout the paper). In order to differentiate central actuators from the ones at the edges, they are shaded in blue. The corners (**1**, **12**, **133**, **144**), although numbered, are positions of zero activity and no actuator is present here (shaded black). The actuator positions shaded in green are called the penultimate actuators here. The behavior of these actuators will be soon shown to be somewhat different from center and edge actuators.

12	24	36	48	60	72	84	96	108	120	132	**144**
11	23	35	47	59	71	83	95	107	119	131	143
10	22	34	46	58	70	82	94	106	118	130	142
9	21	33	45	57	69	81	93	105	117	129	141
8	20	32	44	56	68	80	92	104	116	128	140
7	19	31	43	55	67	79	91	103	115	127	139
6	18	30	42	54	66	78	90	102	114	126	138
5	17	29	41	53	65	77	89	101	113	125	137
4	16	28	40	52	64	76	88	100	112	124	136
3	15	27	39	51	63	75	87	99	111	123	135
2	14	26	38	50	62	74	86	98	110	122	134
1	13	25	37	49	61	73	85	97	109	121	**133**

Figure 2. Actuator Map: Blue region is the central portion and the blackened actuators are the corner actuators, the uncolored region shows the edge actuators and green shaded region depicts penultimate actuators

B. Influence function calculation from SHWS slopes

The influence function was calculated from the SHWS measurements, assuming the slope sensing geometry of Southwell [10] and applying the least square technique. The measured influence functions for the edge, penultimate and central actuators are shown in Fig. 3. It can be observed that the influence functions for each type of actuator (central, edge and penultimate) are different from one other. This is attributed to the presence of the edge and penultimate actuators near the fixed periphery. The systematic error that can be observed on the background in Figs. 3a, 3b and 3c can be remarkably reduced by taking the slope values, measured when 0V is applied to all the actuators, as reference. The background-error-free influence function measurements are shown in Figs. 3d, 3e and 3f.

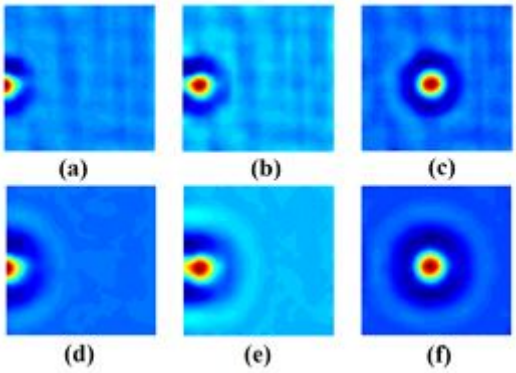

Figure 3. Measured influence function: A poke voltage of 30V is applied to actuators: (a, d) **7**, edge actuator (b, e) **19**, penultimate actuator (c, f) **67**, center actuator, with zeros bias voltage. The surfaces, complete wavefront reconstructions of the DM surface, shown above are each normalized from zero to unity

It is to be remembered that there can be multiple errors involved while sensing the displacement of the DM surface. Apart from the experimental errors due to beam alignment and control, the only other error arises from the inaccuracies in the wavefront sensing algorithm. The experimental errors can be largely minimized by adopting cautious beam control steps. The wavefront sensing algorithm is limited by the wavefront sampling geometry, centroiding algorithm used to detect the position of the SHWS spots and the method used for reconstructing the DM surface from slope measurements.

III. Evaluation of the Inter-Actuator Coupling

The inter-actuator coupling for all the central actuators was evaluated. A histogram of the inter-actuator coupling coefficient (computed for the nearest neighbor) at different voltages for central actuators is shown in Fig. 4. It can be noted here that with increasing poke voltage, the inter-actuator coupling coefficient increases. The inter-actuator coupling coefficient for the next nearest neighbors is very low in the case of central actuators (see Fig. 5). The measured influence function shown in Fig. 3 hints a possible asymmetry in the inter-actuator coupling which is pointed out more convincingly in Fig. 6 for the case of central actuators. Clearly, the actuator coupling is stronger in '*x*' direction.

DOI: 01.IJCSI.03.02.49

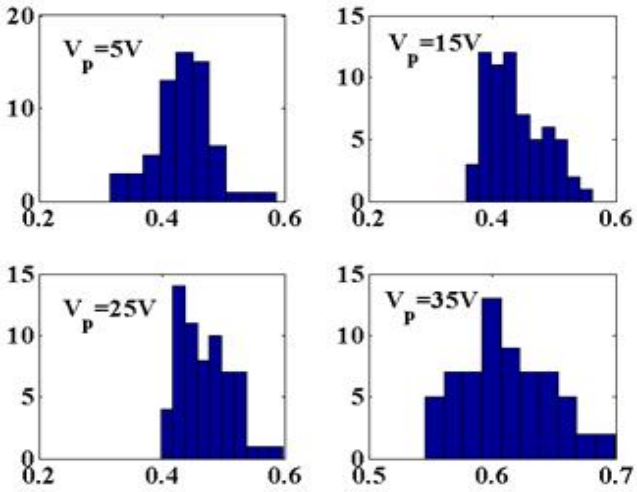

Figure 4. Inter-actuator coupling for the nearest neighbor at different poke voltage. X-axis shows the inter-actuator coupling and Y-axis shows the number of occurrences, analysis on central actuators alone

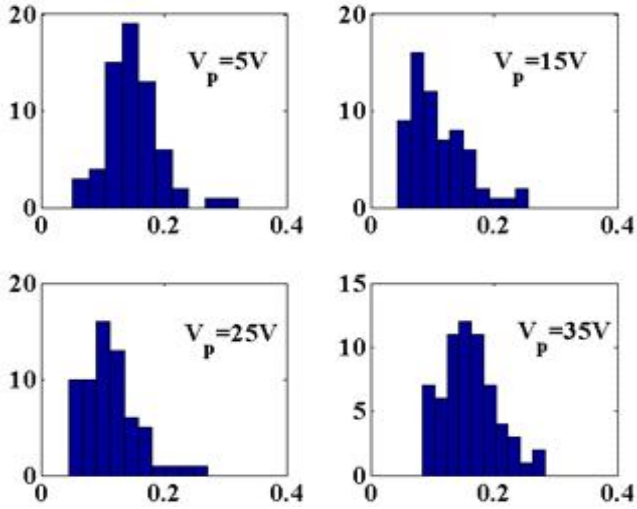

Figure 5. Inter-actuator coupling coefficient for the next nearest neighbor at different poke voltage. X-axis shows the inter-actuator coupling and Y-axis shows the number of occurrences, analysis on central actuators alone

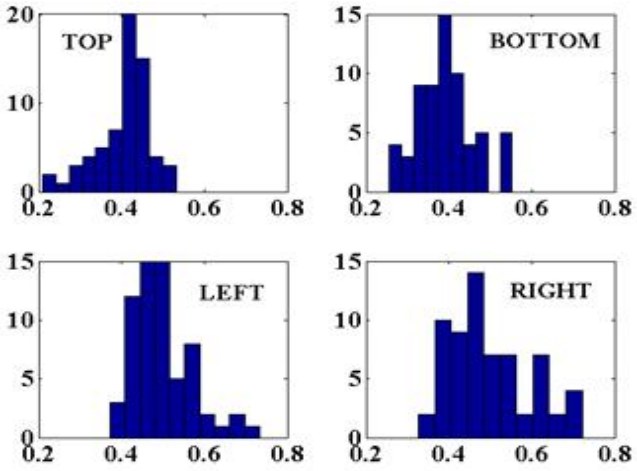

Figure 6. Histogram showing the asymmetry in the inter-actuator coupling along *x* (marked left, right) and *y* (marked top, bottom) directions

IV. Modeling the measured Influence Function

A. Fitting using Zernike polynomials

The measured influence function can also be exactly fitted using the Zernike polynomials, $Z^j(x,y)$ via the calculation of Zernike moments, a^j's:

$$IF(x,y) = \sum_{j=1}^{\infty} a^j Z^j(x,y) \quad (4)$$

Since it is not practical to calculate infinite moments, the influence function is approximated using '*M*' number of finite Zernike moments. The error involved in representing the influence function using a finite number of Zernike moments can be made sufficiently low by choosing a large enough value for '*M*'. Influence function for actuator **66** represented using *M*=75 Zernike moments is shown in Fig. 7. The residual error (see Fig. 7c) is evaluated by subtracting the measured influence function (Fig. 7a) from the fitted model (Fig. 7b) for the influence function.

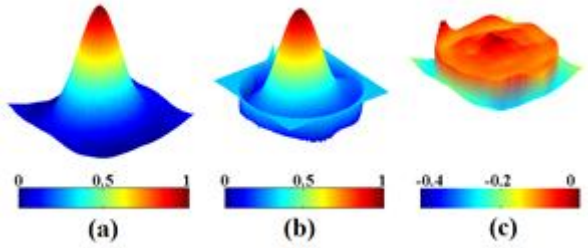

Figure 7. Fit result of actuator **66** with 75 Zernike polynomials with application of a poke voltage, V_p=20V, zero bias (a) Measured influence function (b) Fit function (c) Residual error

Zernike polynomials are defined on the unit disk and the measured influence function is spread over a square grid. This shape incompatibility compelled us to calculate the root mean squared error (RMSE), that determines the fitting accuracy, over one half of the square grid, close to the center alone, excluding the circular boundary where the error is exceedingly large. The value, $\log_{10}$(RMSE) reduces almost linearly with the number of computed Zernike moments up to $j \sim 40$ as can be seen in Fig. 8. Beyond $j > 40$, the reduction continues, but at a smaller rate. This is because the dominant aberrations in the influence function are the lower order Zernikes.

A plot of the Zernike moments for actuators **55, 67** and **77** is shown in Fig. 9. Here, it must be observed that Zernike moments with index, j = 4, 12 and 24 dominate over other Zernike moments for the central actuators. This is because the measured influence functions for central actuators are circularly symmetric, and so are the Zernike polynomials, j = 4, 12 and 24 (see Fig. 12). In the higher spatial frequency range, j = 40, 60 appear to be more different from 0, than the remaining higher order moments. The major drawback in representing the influence function with Zernike polynomials is that the wavefront sensing is performed on a square grid and the representation is done on a unit disk, as is the property of Zernike polynomials. This becomes even more significant while trying to represent an edge actuator.

DOI: 01.IJCSI.03.02.49

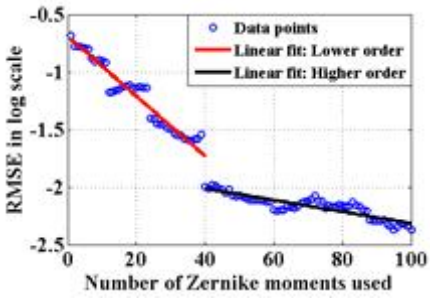

Figure 8. RMSE reduces with increasing number of Zernike moments used for fitting: case of 20V applied to actuator **66** (central actuator), zero bias voltage

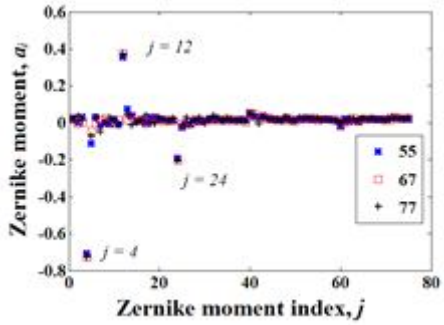

Figure 9. Zernike coefficients on fitting *IF* for actuators **55**, **67**, **79** with a poke voltage of 25V, at zero bias

The edge actuator can be represented with very low residual error using the Zernike moments as shown in Fig. 10. The dominating moments in the case of edge actuators are j = 1, 5 and 6 (see Fig. 11, 12).

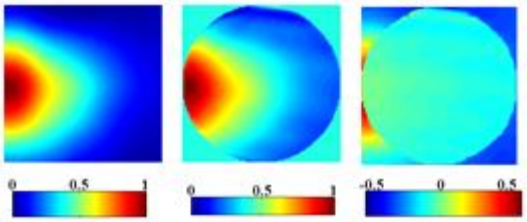

Figure 10. Fit result of edge actuator, **7** with Zernike moments: case of poke voltage of 25V, at zero bias. The residual error is nearly zero in the region where the fitting is done

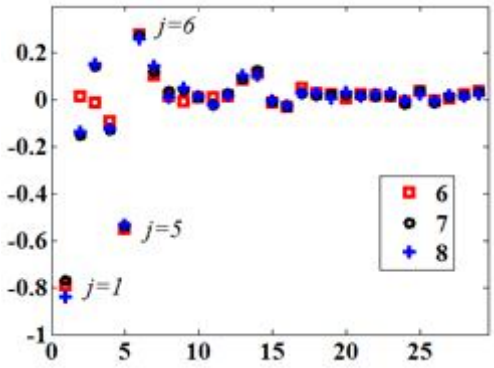

Figure 11. Zernike coefficients on fitting IF for actuators **6**, **7**, **8** with a poke voltage of 25V, at zero bias

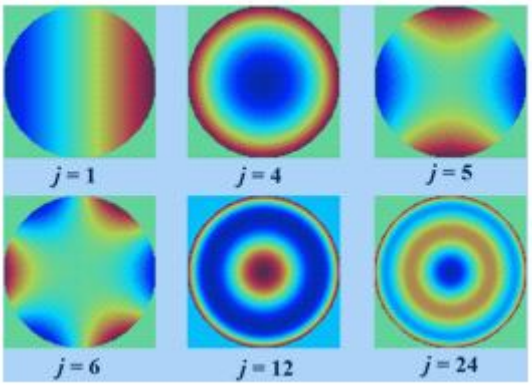

Figure. 12. Zernike polynomials that play vital role in *IF* representation

B. Sinc-squared fit

From the observation of the line profile taken along the X-axis of the measured influence function (*IF*) for actuator **79** as shown in Fig. 13, it can be concluded that the influence function can be modeled as a sinc-squared function. This novel influence function model can be very effectively used to precisely represent the response of individual actuators.

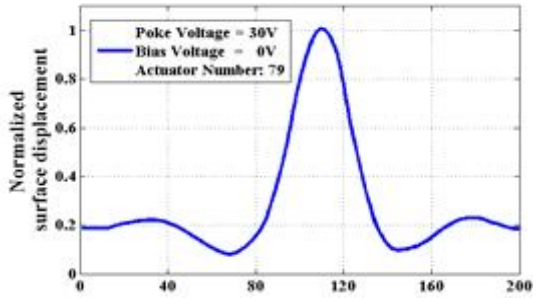

Figure 13. Line profile (1D view) of the measured influence function

In the 2D case, a most general sinc-squared model of the influence function model can be expressed,

$$IF^{\text{model}}(x,y) = a_0 + a_1\left[\begin{array}{l}\text{sinc}\left(\frac{x}{s_x}+c_x\right)\times\text{sinc}\left(\frac{y}{s_y}+c_y\right)\\ \times\,\text{sinc}\left(\frac{xy}{s_{xy}}+c_{xy}\right)+d\end{array}\right]^2 \qquad (2)$$

or by neglecting the cross term, it can become,

$$IF^{\text{model}}(x,y) = a_0 + a_1\left[\text{sinc}\left(\frac{x}{s_x}+c_x\right)\times\text{sinc}\left(\frac{y}{s_y}+c_y\right)+d\right]^2 \qquad (3)$$

where, a_0, a_1, s_x, c_x, s_y, c_y, s_{xy}, c_{xy} and d are the fitting parameters. Looking at the Eqs. (2) and (3), the assumed model for the influence function certainly looks complicated with the need to estimate multiple parameters, nine and seven in number respectively. The expression in Eq. (3) can be further simplified by considering c_x and c_y to be identically equal to zero, in those cases where this approximation to the influence function remains valid. The trust-region reflective Newton method (large-scale) was used for the optimization of the fitting parameters. A central actuator, **78** was fitted using this

DOI: 01.IJCSI.03.02.49

method and it was found that the residual error is very low (see Fig. 14). R-square, that measures the success of the fit via the calculation of the correlation between the measured influence function and the fitted model, is used as a metric that determines the fit accuracy and in this case, it is 0.9901. The motivation behind favoring sinc-squared instead of sinc function is that with the former, the fitting root mean square error (RMSE) is lesser by a factor of 5, than that of the later. It was also noted that, in comparison with the Gaussian fitting, [see Eq. (1)] the sinc-squared fitting [see Eq. (2)] improves the R-square value by a factor of 1.8. In the case of central actuators, the cross term in Eq. (2) can further improve the fitting accuracy, but the increase in fit accuracy is too small (R-square is greater by 0.02) and does not significantly affect our modeling and hence may be ignored and Eq. (3) can be used for simplicity.

The values of '*x*' and '*y*' were chosen to be positive integers alone, while using the sinc-squared model of influence function, in the case of edge actuators (see Fig. 15). It was observed that retaining the cross term in the case of edge actuators and penultimate actuators leads to erroneous fitting and hence Eq. (3) was used for edge actuator modeling.

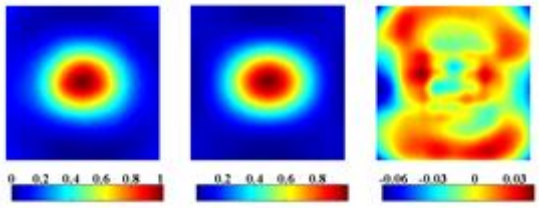

Figure 14. Fit result of central actuator **78** with sinc functions with application of 20V, at zero bias

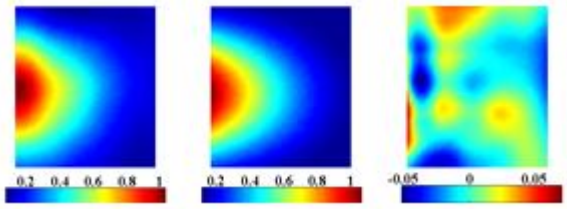

Figure 15. Fit result of edge actuator **7** with Eq. (3): case of poke voltage of 25V, at zero bias. Here, c_x, c_y take non-zero values

It was found that for the central actuators, the median of the R-square value for fitting the sin-squared function in Eq. (2) is just above 0.98. Also, for the central actuators, the medians of a_0, c_x, c_y, c_{xy} are 0.0388, 0.0145, 0.0276 and -0.0049 and hence may be approximated to zero. This observation allows us to reduce Eq. (2) into a 5-parameter optimization problem. From our observations, the most probable model of the DM using the sinc-squared function as defined in Eq. (2) is:

$$IF^{\text{model}}(x,y) = 0.63\left[\begin{array}{c}\text{sinc}\left(\frac{x}{0.74}\right)\times\text{sinc}\left(\frac{y}{0.92}\right)\\ \times\text{sinc}\left(\frac{xy}{0.65}\right)+0.27\end{array}\right]^2 \quad (4)$$

Conclusions

In this paper, a novel model for the measured influence function of a continuous DM is presented. The sinc-squared function can be used to closely model the influence function. It is indicated that the behavior of the edge actuators and penultimate actuators is not the same as that of the central actuator which is made clear with the domination of different Zernike modes in each of the cases. The inter-actuator coupling coefficient increases as the poke voltage increases. The most affected actuator is the nearest neighbor and the next nearest neighbor is affected a little too. There is asymmetry in the inter-actuator coupling coefficient in different directions. Actuator modeling is better with sinc-squared function due to the requirement of circular aperture for representation in terms of Zernike polynomials. The current analysis will gain more significance when the DM is used in an optical layout for wavefront correction accommodating the modeled influence function.

References

[1] T. G. Bifano, J. Perreault, M. R. Krishnamoorthy, M. N. Horenstein, "Microelectromechanical deformable mirrors," *IEEE Journal of Selected Topics in Quantum Electronics*, vol.5, no.1, pp. 83-89, Jan/Feb 1999.

[2] Dani Guzmán, Francisco Javier de Cos Juez, Fernando Sánchez Lasheras, Richard Myers, and Laura Young, "Deformable mirror model for open-loop adaptive optics using multivariate adaptive regression splines," *Opt. Express*, 18, 6492-6505 (2010).

[3] Michael Shaw, Simon Hall, Steven Knox, Richard Stevens, and Carl Paterson, "Characterization of deformable mirrors for spherical aberration correction in optical sectioning microscopy, " *Opt. Express*, 18, 6900-6913 (2010).

[4] R. G. Lane and M. Tallon, "Wave-front reconstruction using a Shack-Hartmann sensor," *Appl. Opt.*, 31, pp. 6902-6908, 1992.

[5] Wenhan Jiang, Ning Ling, Xuejun Rao and Fan Shi, "Fitting capability of deformable mirror", *Proc. SPIE* 1542, 130, 1991.

[6] Linhai Huang, Changhui Rao, and Wenhan Jiang, "Modified Gaussian influence function of deformable mirror actuators," *Opt. Express*, 16, pp. 108-114, 2008.

[7] J. H. Lee, T. K. Uhm, S. K. Youn, "First-Order Analysis of Thin-Plate Deformable Mirrors," Journal of the Korean Physical Society, Vol. 44, No. 6, pp. 1412-1416, 2004.

[8] M. B. Roopashree, A. Vyas, and B. R. Prasad, "Automated ROI selection and calibration of a microlens array using a MEMS CDM," in *Adaptive Optics: Methods, Analysis and Applications, OSA Technical Digest (CD)* (Optical Society of America, 2011), paper ATuA5.

[9] M. B. Roopashree, A. Vyas, and B. R. Prasad, "Experimental evaluation of centroiding algorithms at different light intensity and noise levels," *AIP Conf. Proc.*, to be published.

[10] W. H. Southwell, "Wave-front estimation from wave-front slope measurements," *J. Opt. Soc. Am.*, 70, pp. 998-1006, 1980.

DOI: 01.IJCSI.03.02.49